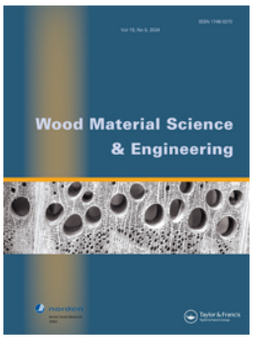

Wood Material Science & Engineering

ISSN: (Print) (Online) Journal homepage: www.tandfonline.com/journals/swoo20

Lead ion adsorption by biochar manufactured from downed timber: the effect of downed timber maturity and environmental exposure period

Yucheng Peng, Ruiqi Li, Muhammad Irfan, Shaoyang Liu, Dengjun Wang, Thomas Elder, Qiangu Yan & Zhiyong Cai

To cite this article: Yucheng Peng, Ruiqi Li, Muhammad Irfan, Shaoyang Liu, Dengjun Wang, Thomas Elder, Qiangu Yan & Zhiyong Cai (21 Nov 2024): Lead ion adsorption by biochar manufactured from downed timber: the effect of downed timber maturity and environmental exposure period, Wood Material Science & Engineering, DOI: 10.1080/17480272.2024.2431168

To link to this article: https://doi.org/10.1080/17480272.2024.2431168

Published online: 21 Nov 2024.

WOOD MATERIAL SCIENCE & ENGINEERING
https://doi.org/10.1080/17480272.2024.2431168

Taylor & Francis
Taylor & Francis Group

ORIGINAL ARTICLE

Lead ion adsorption by biochar manufactured from downed timber: the effect of downed timber maturity and environmental exposure period

Yucheng Peng[a], Ruiqi Li[a], Muhammad Irfan[a], Shaoyang Liu[b], Dengjun Wang[c], Thomas Elder[d], Qiangu Yan[e] and Zhiyong Cai[e]

[a]College of Forestry, Wildlife, and Environment, Auburn University, Auburn, AL, USA; [b]Center for Materials and Manufacturing Sciences, Department of Chemistry and Physics, Troy University, Troy, AL, USA; [c]School of Fisheries, Aquaculture and Aquatic Sciences, Auburn University, Auburn, AL, USA; [d]Southern Research Station, USDA-Forest Service, Auburn, AL, USA; [e]Forest Products Laboratory, USDA-Forest Service, Madison, WI, USA

ABSTRACT

Downed timber is valuable for manufacturing biochar in environmental remediation applications due to the low cost of raw materials and low-temperature manufacturing process. Loblolly pine (*Pinus taeda* L.) trees at different maturities (15-, 30-, and 39-year-old) with 0, 6, and 12 months of local environmental exposure in the southeastern region of the US were collected for biochar manufacturing. The biochar samples were characterized for their physicochemical properties, including morphologies, elemental compositions, surface functional groups, carbon structure, pH, electrical conductivity, and specific surface area. The Pb^{2+} adsorption isotherms were measured. The results indicated that the biochar physicochemical properties, affected by the tree maturities and the environmental exposure periods, significantly impacted the Pb^{2+} adsorption capacity. The Pb^{2+} adsorption capacity of biochar increased with the environmental exposure of wood for 6 months, followed by a decrease for biochar made from wood with an environmental exposure of 12 months. A recommendation can be made that downed timber collected up to a 6-month environmental exposure period can manufacture biochar with superior performance regarding adsorbing Pb^{2+} in water systems. The research outcome offered insights for the biochar manufacturing community to prepare forest feedstock for biochar production with better performance in Pb^{2+} adsorption.

ARTICLE HISTORY
Received 12 September 2024
Accepted 13 November 2024

KEYWORDS
Downed timber; biochar; pH; electrical conductivity; lead ion; adsorption

Introduction

Available freshwater resources are decreasing due to world population growth, rapidly developing industries, increasing urbanization, exhaustive natural resources exploitation, long-time droughts, and often occurrences of extreme weather (Carolin *et al.* 2017, Vardhan *et al.* 2019, Zamora-Ledezma *et al.* 2021, Mahmoud *et al.* 2023, Olsen *et al.* 2023). Additional contamination of water resources with pollutants resulting from human activity and natural events, like volcanoes, earthquakes, or storms, worsen the water shortage even in rich water supply regions (Stewart *et al.* 2006, Uprety *et al.* 2017, Villarín and Merel 2020, Zamora-Ledezma *et al.* 2021). Among the pollutants released from natural and anthropogenic sources, heavy metal contaminants in freshwater resources are a long-existing and ever-evolving threat to human health and the ecosystem (Kurniawan *et al.* 2006, Fu and Wang 2011, Gautam *et al.* 2015, Inyang *et al.* 2016, Shaheen *et al.* 2019, Chai *et al.* 2021, Abdullaev *et al.* 2023). Due to the broad applications and wide existence in the earth's crust of heavy metals, they can enter the environment through a variety of anthropogenic sources as well as from the natural geochemical weathering of soil and rocks. The main sources of heavy metal contaminants in anthropogenic sources include mining wastes, landfill leachates, municipal wastewater, urban runoff, and industrial wastewater, particularly wastewater generated from the electroplating, electronic, and metal-finishing industries (Gautam *et al.* 2015). A study indicated that approximately 40% of the lakes and rivers of the planet have been polluted by heavy metals (Zhou *et al.* 2020).

Removing heavy metals from the water system is important, and many technologies have been developed to address this issue. The methods reported in the literature include various treatments with the heavy metal removing mechanisms of precipitation and coagulation, ion exchange, membrane filtration, bioremediation, heterogeneous photocatalytic degradation, and adsorption (Fu and Wang 2011, Chai *et al.* 2021, Sharma *et al.* 2022). Among these methods, adsorption is one of the most cost-effective methods for the remediation of heavy metals in water (Inyang *et al.* 2016, Yang *et al.* 2019). The adsorption process using an adsorbent with a highly porous structure has a low operating cost, high removal capacity, and easy implementation (Shaheen *et al.* 2019, Yang *et al.* 2019, Qasem *et al.* 2021). Various adsorbent systems have been widely investigated, including biosorbents, magnetic adsorbents, mineral adsorbents, metal–organic framework adsorbents, and activated carbon-based adsorbents (Duan *et al.* 2020, Qasem *et al.* 2021). Each adsorbent system has advantages and disadvantages, and novel adsorbent systems with lower production and implementation costs and environmentally friendly characteristics are still needed.

As an efficient, cost-effective, and environmentally friendly adsorbent manufactured from renewable forest feedstock,

CONTACT Yucheng Peng yzp0027@auburn.edu College of Forestry, Wildlife, and Environment, Auburn University, 602 Duncan Drive, Auburn, AL 36849, USA

biochar has great potential to mitigate heavy metal contamination (Inyang *et al.* 2016, Shaheen *et al.* 2019, Wang *et al.* 2020). Following decades of expansion, forest and woodland areas in the U.S. have plateaued at 333 million hectares. Around 3% of the forest land in the U.S. is disturbed yearly by natural events such as insects, disease, and fire, which is more than annual removals (less than 2%) (Oswalt *et al.* 2019). Utilizing these biomass resources disturbed by natural events has been considered for its potential to help offset the cost of reducing wildfire hazards, promoting forest regeneration, and restoring forest resilience (Schoennagel *et al.* 2004, Weaver *et al.* 2009, Svoboda *et al.* 2010, Freschet *et al.* 2013, Woodall *et al.* 2013). Manufacturing biochar from these damaged wood resources (downed timer) for value-added applications of mitigation of heavy metal contaminants also provides additional opportunities for the landowner to offset the damage caused by natural disturbances. Research also indicated that manufacturing biochar from waste wood is a global perspective, and biochar from wood can outperform other chars due to relatively high porosity (Marousek and Trakal 2022).

The use of downed timber for biochar manufacturing has two concerns that need to be considered for producing products with consistent qualities and performance. Firstly, downed timber generated by natural disturbances includes wood resources of a variety of ages. After natural disturbances, wood with different properties and various chemical compositions can be salvaged (juvenile versus mature wood). A 40-year-old loblolly pine tree contains approximately 15% juvenile wood, while a 15-year-old tree has around 85% juvenile wood (Yeh 2006). Juvenile pine wood generally has a larger proportion of earlywood, more extractives, smaller specific gravities, shorter tracheid lengths, and larger fibril angles than mature wood (Larson *et al.* 2001). These characteristic differences between juvenile wood and mature wood would pose potential inconsistent properties of the biochar obtained. Simultaneously, juvenile wood contains more lignin and less cellulose than mature wood (Lu *et al.* 2021). The biochar products generated from juvenile wood are expected to differ from mature wood due to the different contents of the major polymer chemical components and the microscopic wood structures (Collard and Blin 2014, Tomczyk *et al.* 2020).

The second concern of producing biochar from downed timber is associated with the length of time between its collection and the event that caused the disturbance. Degradation of downed timber changes with time, local weather, and environmental conditions. Several stages of wood degradation progress along the extended environmental exposure period (Goodell *et al.* 2020). Microorganisms, insects, and moisture are the major factors contributing to the degradation of wood. With appropriate environmental conditions, fungi mainly cause changes in wood quality and chemical composition. Different chemical composition changes can result depending on the specific categories of fungi. For example, two main wood rot fungus categories that cause considerable degradation are white rot and brown rot fungi (Rayner and Boddy 1988), which grow most rapidly at the temperature range of 20 – 32 °C (Shmulsky and Jones 2019). White rot fungi are mostly associated with hardwoods but can be found in softwoods (Krah *et al.* 2018). Most of the white rot fungi can depolymerize all three cell wall polymers (cellulose, hemicellulose, and lignin) simultaneously, while some selective white rot fungi can preferentially digest the hemicellulose and lignin components, leaving much of the crystalline cellulose relatively undegraded (Goodell *et al.* 2020). Brown rot fungi are mainly associated with softwoods, decomposing cellulose and hemicellulose, but not lignin (Goodell *et al.* 2020). Therefore, downed and degraded timber collected at different times may contain different chemical components. The thermochemical conversion mechanisms for each polymer component, i.e. cellulose, hemicellulose, and lignin, are also significantly different, and different biochar yields and porous structures will be obtained (Collard and Blin 2014) depending on the degrees of downed timber degradation. The ratios of the three polymers also affect the biochar production process (Collard and Blin 2014). Therefore, biochar produced from downed timber differs in structure and performance, and the significance of the differences in the potential applications of biochar in removing heavy metals needs to be evaluated.

The objective of this study is to evaluate the biochar manufactured from downed timber with different tree maturities and environmental exposure periods in terms of physicochemical properties and heavy metal adsorption capacities. In this study, loblolly pine (*Pinus taeda* L.) trees of different ages were felled and exposed to the environment for different periods of time. The biochar samples were produced in the laboratory using a controlled pyrolysis procedure. The physicochemical properties of the biochar that were determined were morphology, pH, electrical conductivity (EC), surface functional group composition, elemental composition, and lead ion adsorption capacity. The effect of tree age and environmental exposure period on biochar properties and lead ion adsorption capacities was evaluated. The hypothesis is that the biochar behaviors in adsorbing lead ions vary significantly among different biochar samples, and the lead ion adsorption capacities are impacted by the physicochemical characteristics.

Experimental

Materials

Three loblolly pine (*Pinus taeda* L.) trees aged 15, 30, and 39 years old (denoted as L15, L30, and L39, respectively) were selectively felled on October 22, 2020, at the Solon Dixon Forestry Education Center, Andalusia, AL. The exact locations of the three trees can be found in our previous publication (Peng *et al.* 2024). The three trees were cut to be left in the natural environment with a stump height of around 30 cm. Wood log samples with a length of 15 – 30 cm were then collected from the bottom of each tree on November 3, 2020, April 23, 2021, and October 1, 2021, to include samples covering a year of environmental exposure. After collection, all the wood log samples were stored in a freezer at −20 °C for the next step of operation. Lead (II) chloride ($PbCl_2$) at a purity of 99% (Chemical identifier number: CAS) was purchased from VWR International (Radnor, PA, USA).

Biochar preparation

The loblolly pine wood log samples were debarked, and the size was reduced using a table saw to be fed into a chipper (Brush Master chipper shredder CH11, Maple Grove, MN, USA) to manufacture wood chips. The wood chips were dried overnight at 105 °C in an oven and stored in Ziploc bags for biochar manufacturing.

Biochar from the loblolly pine wood chips was prepared using a quartz tube furnace (GSL-1100X, MTI Corporation, Richmond, CA, USA) under nitrogen gas. The temperature profile used for biochar manufacturing included four steps: 1) ramping temperature from room temperature to 450 °C at 10 °C /min, 2) holding temperature at 450 °C for one hour, 3) cooling at 10 °C/min to 200 °C, and 4) cooling from 200 °C to room temperature naturally. After cooling to room temperature, the biochar samples were collected in a high-density polyethylene container with a cap on. The biochar samples produced from log samples collected in November 2020 are denoted as L15-0M, L30-0M, and L39-0M. Similarly, the biochar samples L30-6M and L39-12M indicated that the biochar samples were produced from log samples collected in April 2021 and October 2021 from L30 and L39, respectively. A similar nomenclature style was employed to denote all the other biochar samples.

Biochar characterization

Scanning electron microscopy characterization of a small section of the biochar samples manufactured from wood chips was performed using a Zeiss Evo 50VP scanning electron microscope (Oberkochen, Germany) operated at an accelerating voltage of 20 kV. The pH and EC of the biochar samples were determined in a biochar suspension with the biochar to deionized water weight ratio of 1:10 (Singh *et al.* 2017). The biochar suspension was prepared by adding 1.5 grams of biochar particles (obtained by grinding biochar manufactured from wood chips into smaller particles using a set of mortar and pestle followed by sieving to collect biochar particles smaller than 2 mm) into 15 mL of deionized water in a 50 mL centrifuge tubes. The suspension was then mixed using a Scilogex Sci-RL-E tube rotator (Rocky Hill, CT, USA) with a rotating speed of 20 rpm for one hour, followed by standing for 30 min. The pH and EC of biochar samples were measured using an Extech EC600 pH and digital conductivity meter (Waltham, MA, USA). Before measurement, the pH meter was calibrated using buffer solutions of pH 4, 7, and 10, while the EC meter was calibrated using a buffer solution of 1413 µs/cm. The measurements of pH and EC were performed in triplicate, and the average values were reported.

The powder form biochar samples for all the other characterizations were prepared by ball milling (PTA-02 Model, Nidec Shimpo Corporation, Japan). The ball milling process was conducted for seven hours at 180 rpm using a 5 L porcelain jar loaded with 40 cylindrical porcelain milling media with a diameter of 12.7 mm and a height of 12.7 mm. After ball milling, biochar powers with particle sizes smaller than 106 µm were collected for characterization. Fourier transformation infrared spectroscopy (FT-IR) was used to characterize the surface functional groups of the biochar samples using a PerkinElmer Spectrum Two FT-IR spectrometer (Waltham, MA, USA) equipped with an attenuated total reflection (ATR) accessory. All spectra were taken via the ATR accessory in the wavenumber range of 650 – 4000 cm^{-1} with 128 scans and a resolution of 4 cm^{-1}. Three replicates were collected for each biochar sample. All the data analyses on the spectra were performed using Spectrum 6 spectroscopy software (PerkinElmer, MA, USA). A Raman spectrometer equipped with a 785-nm laser (MacroRAM, Horiba Scientific, Piscataway, NJ, USA) was employed to acquire the spectrum in a Raman shift range of 150–3250 cm^{-1} for all the biochar samples. Three replicates were collected for each biochar sample. The elemental compositions of the biochar samples were determined using an elemental analyzer (Thermo Scientific FLASH 2000 CHNO analyzers, Waltham, MA, USA) on the power form biochar samples, and oxygen content was determined by the difference of total sample weight with the contents of C, N, and H.

The gas adsorption isotherms of CO_2 on the biochar samples were measured by CO_2 physisorption at 0 °C using a Micromeritics TriStar II Plus instrument (Norcross, GA, USA) in the pressure range from 1.33 x 10^2 to 1.01x10^5 Pascal that corresponds to (approximately 4 x 10^{-5} to 0.029 P/P_0) for CO_2. The gas adsorption isotherm of N_2 was also tried to obtain for the biochar samples. No consistent results were achieved for N_2 adsorption. Therefore, only CO_2 adsorption isotherms were studied in this research. Before the gas adsorption measurement, the biochar samples were degassed under a vacuum at 300 °C for 24 h using a VacPrep 061 instrument (Micromeritics, Norcross, GA, USA). Two replicates were performed for the CO_2 adsorption to obtain the isotherms. The CO_2 adsorption isotherms were fitted with the Dubinin-Astakhov equation (Dubinin and Stoeckli 1980, Chen and Yang 1994, Hutson and Yang 1997, Hu and Ruckenstein 2006) shown below:

$$\log(V) = \log(V_0) - \left[\frac{RT}{\beta E_0}\right]^n \left[\log\left(\frac{p_0}{p}\right)\right]^n \quad (1)$$

where p, p_0, V, V_0, n, R, E_0, and β are the equilibrium pressure, the saturation vapor pressure of CO_2 at the analysis temperature (T), the volume adsorbed at equilibrium pressure (p), the monolayer capacity, the Astakhov exponent, the gas constant, characteristic energy, and the affinity coefficient of CO_2 (0.46) (Carrascomarin *et al.* 1993), respectively. The monolayer adsorption capacity (V_0), Astakhov exponent (n), and characteristic energy (E_0) for all the biochar samples were reported according to the data analysis on CO_2 adsorption isotherms. The specific surface area (SSA) of the biochar samples in m^2/g was then calculated as:

$$SSA = \frac{6.203 \times 10^{23} \sigma V_0}{22414 \times 10^{18}} \quad (2)$$

where σ is the molecular sectional area of CO_2 at 0 °C (0.187 nm^2)(Carrascomarin *et al.* 1993). The SSAs for all the biochar samples were reported.

Lead ion adsorption isotherm

The lead (II) ion (Pb^{2+}) adsorption capacities of the biochar samples were calculated by fitting the Pb^{2+} adsorption isotherms for all the biochar samples measured in solutions using Langmuir adsorption isotherm model. In this study, the $PbCl_2$ solutions at different concentrations were prepared by mixing solid $PbCl_2$ in deionized water, and the concentration of Pb^{2+} was determined using an ultraviolet/visible (UV/Vis) spectrophotometer (UV-1600PC, VWR, Radnor, PA, USA). A calibration curve was established to correlate the intensity of the UV wavelength at 208 nm with the Pb^{2+} concentrations prepared in the laboratory with Pb^{2+} concentrations in the range of 1 – 30 mg/L.

The Pb^{2+} adsorption isotherms for all the biochar samples were collected by adding 40 mg of biochar to 20 mL Pb^{2+} solutions in polypropylene centrifuge tubes at concentrations of 10, 20, 30, 40, 50, 60, and 70 mg/L, followed by mixing using a Scilogex Sci-RL-E tube rotator (Rocky Hill, CT, USA) with a rotating speed of 40 rpm for three days. After mixing, the solutions were extracted using syringes and filtered with a 0.45 µm PTFE membrane. The solution without biochar was then diluted with several trials to measure the Pb^{2+} concentration within the 1 – 30 mg/L range. The adsorption isotherm representing the relationship between the amount of Pb^{2+} adsorbed on the biochar surface in (mg/g) and the Pb^{2+} concentrations in water (mg/L) was generated. The Langmuir model in the linear form shown in equation (3) was used to fit the isothermal data for calculating the Pb^{2+} adsorption capacity (Chen *et al.* 2022).

$$\frac{C_e}{q_e} = \frac{C_e}{q_m} + \frac{1}{K_L\, q_m} \tag{3}$$

where C_e, q_e, q_m, and K_L are the equilibrium concentration of Pb^{2+} in solution, the amount of adsorption on biochar at equilibrium, the maximum adsorption capacity, and Langmuir isotherm constant.

Statistical analysis

Statistical analysis of the quantitative data obtained in this study was performed to understand the effect of the two factors at three levels, including tree maturities (15, 30, and 39 years old) and environmental exposure periods (0, 6, and 12 months), on the biochar physicochemical properties and lead ion adsorption capacities. A two-way analysis of variance (ANOVA) with a 0.05 significance level was conducted. A statistical model was used to represent the mean value of the quantitative data of the biochar samples impacted by tree maturity ($\alpha = 1$, 2, and 3 representing 15, 30, and 39 years old) and environmental exposure period ($\beta = 1$, 2, and 3 representing 0, 6, and 12 months) as shown in equation 4.

$$Y_{ijk} = \mu + \alpha_i + \beta_j + (\alpha\beta)_{ij} + e_{ijk} \tag{4}$$

where $i = 1, 2, 3$; $j = 1, 3, 3$; and $k = 1, 2, 3$. The measured mean values (Y_{ijk}) is a function of population mean data (μ) of the biochar samples, impact by tree maturity (α_i), environmental exposure period (β_j), and the interactions between the two factors ($(\alpha\beta)_{ij}$) plus the errors in the model (e_{ijk}) which is assumed to be independently, identically, and normally distributed. Following the ANOVA analysis, a post-hoc test using Tukey's Honestly Significant Different (TukeyHSD) test was employed to understand the effect of different fact levels with each group.

Results and discussions

Biochar morphologies

The SEM micrographs at different magnifications demonstrating the morphologies of the biochar from the loblolly pine trees at different tree maturities are shown in Figure 1. After pyrolysis using the conditions in this study, all the biochar samples preserved the original wood structures, and biochar converted from earlywood and latewood can be easily identified for all three different tree maturities. Continuous structures with a much thicker wall in latewood biochar than in earlywood biochar are demonstrated in Figure 1. Other structural characteristics of the loblolly pine tree, including resin canal, rays, and pit pairs, can also be observed in the biochar samples. From the SEM micrographs, no obvious difference in biochar structures can be observed among different tree maturities. Within the same tree age group, the morphologies of biochar samples converted from the wood chips with different environmental exposure periods were also evaluated, and a similar case was also noted. It is inconclusive to distinguish biochar samples from different tree maturities and environmental exposure periods based on SEM micrographs.

Biochar elemental compositions

The C, H, and O compositions of the biochar samples were measured, and the data are shown in Table 1. The ratios of O to C for all the biochar samples are also calculated and included in the table. After pyrolysis, the biochar samples manufactured from three different ages of loblolly pine trees have C contents of 82.0 ± 1.9, 84.4 ± 3.9, and 85.0 ± 0.3%. Within the group of biochar samples made from a 15-year-old tree, the C contents are 82.0 ± 1.9, 84.8 ± 1.2, and 84.0 ± 0.8 % with an environmental exposure period of 0, 6, and 12 months, respectively. For the group of L30 biochar samples, the C contents changed from 84.4 ± 3.9 for the 0-month sample to 83.4 ± 0.2 and 82.6 ± 0.3 % for the samples with 6 and 12 months of environmental exposure, respectively. Statistical analysis of the C contents of the biochar samples was performed, and the results indicated that there was no significant interaction effect for the two factors – tree maturity and environmental exposure – on the biochar sample C contents. No significant effect of tree maturity on biochar C contents was also observed using the TukeyHSD test. Within each tree maturity group, the environmental exposure period was also not found to impact the C contents of biochar samples significantly. The H content in all the biochar samples ranged from 3.5 ± 0.1 to 3.8 ± 0.1 %, and statistical analysis showed that there was no significant difference among all the biochar samples. The O contents of the biochar samples were calculated as the difference between biochar mass and the O and H contents, and the data ranged from 10.9 ± 1.3 to 14.6 ± 1.8%. The O to C ratios were also calculated and ranged from 12.8±0.1 to 17.9

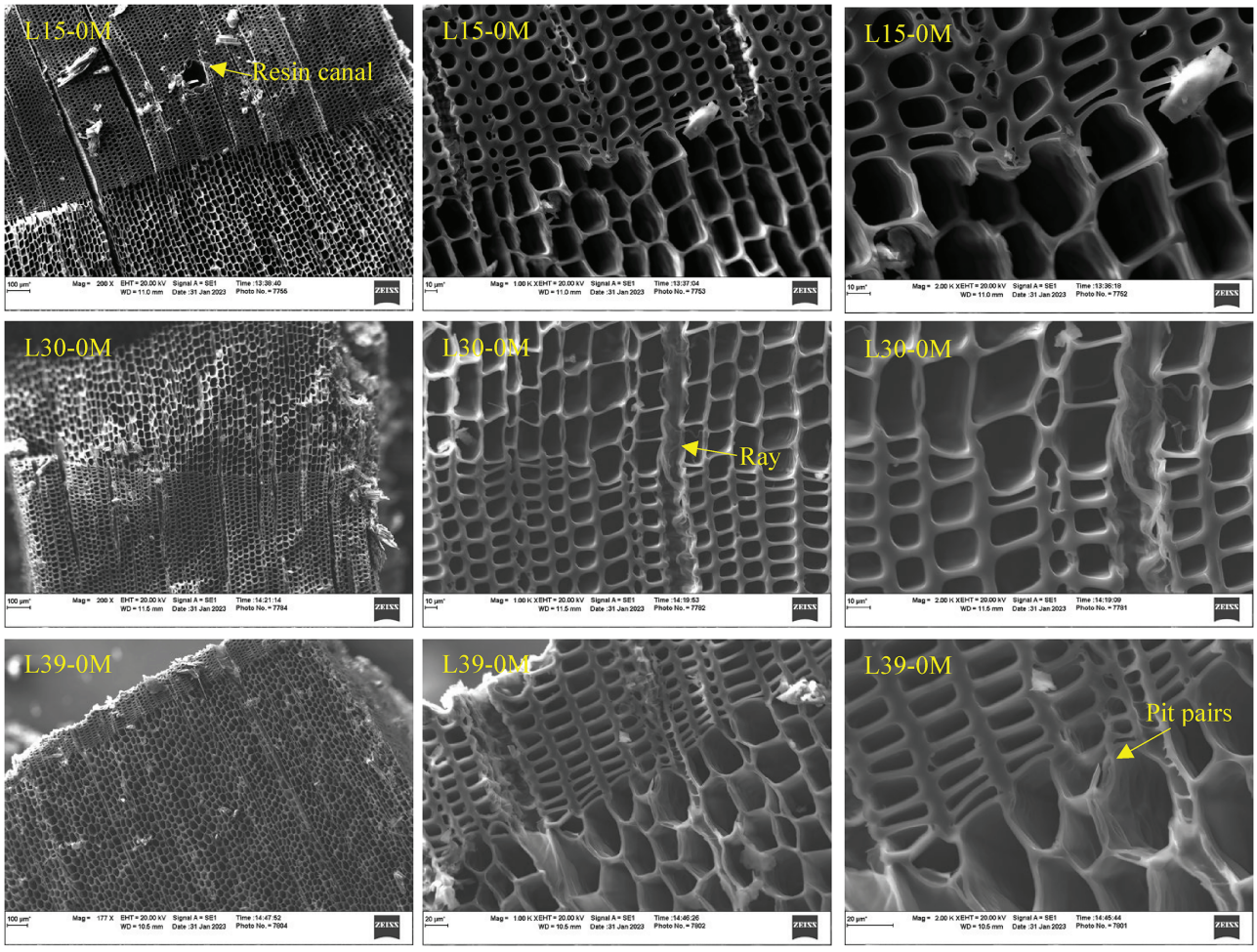

Figure 1. The SEM micrographs at various magnifications for the biochar samples manufactured from loblolly pine trees at three different ages.

Table 1. The C, H, and O compositions of biochar samples.

	C (%)			H (%)			O (%)			O:C (%)		
Sample	0M	6M	12M	0M	6M	12M	0M	6M	12M	0M	6M	12M
L15	82.0±1.9	84.8±1.2	84.0±0.8	3.5±0.1	3.7±0.1	3.6±1.2	14.6±1.8	11.6±1.2	12.4±0.8	17.9±0.1	13.7±0.1	14.8±0.1
L30	84.4±3.9	83.4±0.2	82.6±0.3	3.6±0.1	3.6±0.1	3.5±0.1	12.0±4.0	13.0±0.3	13.9±0.3	14.4±0.1	15.6±0.1	16.9±0.1
L39	85.0±0.3	84.2±1.8	85.3±1.3	3.6±0.1	3.6±0.1	3.8±0.1	11.4±0.4	12.2±1.8	10.9±1.3	13.4±0.1	14.5±0.1	12.8±0.1

±0.1%. The statistical analysis indicated that there was no significant difference in the O contents and the O to C ratios for all the biochar samples. After pyrolysis, the two factors, including the tree maturity and environmental exposure period, have no significant impact on the biochar sample elemental compositions, including C, H, and O contents.

Biochar surface functional groups and carbon-based structure

The FT-IR spectra of the biochar samples from loblolly pine trees at different ages (ages 15, 30, and 39) and the same environmental exposure (0 months) are shown in Figure 2. The surface functional groups of the biochar samples were identified by comparing the obtained FT-IR spectra with the literature data (Han *et al.* 2013, Mukome *et al.* 2013, Li *et al.* 2019, Bandara *et al.* 2020, Wang *et al.* 2022), and the peak assignments are summarized in Table 2. Peak #1, located in the region between 1700 and 1695 cm^{-1}, is attributed to the C = O vibration in the carboxylic group (Han *et al.* 2013,

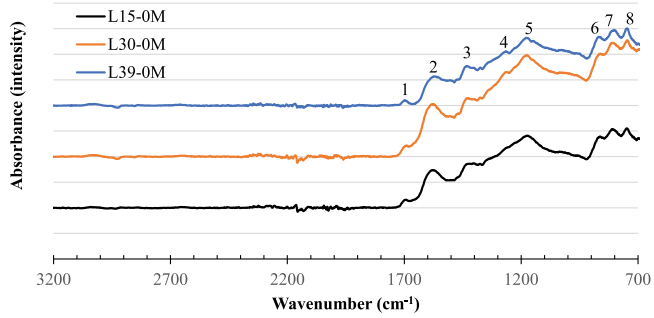

Figure 2. The FT-IR spectra of biochar samples manufactured from wood at ages 15, 30, and 39 collected in October 2020 (The peaks from 1 to 8 were identified in Table 2).

Table 2. The functional groups of biochar samples characterized by FT-IR.

Peak No.	Wavenumber (cm^{-1})	Peak assignments
1	1697	C = O from carboxylic acids, amides, esters and ketones
2	1580	Aromatic C = C stretching
3	1435	C-H in aliphatic carbon (CH_2)
4	1270	Carboxylic acid C-O stretch, carboxyl, ester/ amide region
5	1180	C-O lignin
6, 7, 8	860, 810, 743	Aromatic C-H bond

Mukome *et al.* 2013, Bandara *et al.* 2020). Peak #2 is identified as aromatic C = C stretching at approximately 1582 cm^{-1} (Han *et al.* 2013, Li *et al.* 2019). Peak #3 (1435 cm-1) is the signal of C–H in aliphatic carbon CH_2, correlated with the amorphous region of biochar (Bansal and Goyal 2005, Shin *et al.* 2015). The peaks of 4 (1270 cm^{-1}) and 5 (1180 cm^{-1}) are ascribed to asymmetric stretching of C–O bond in carboxylic acid and lignin, respectively. The aromatic nature of the biochar samples was also indicated by the peaks at 860, 810, and 743 cm^{-1} (peaks 6, 7, and 8), which are attributed to the bending of C–H bonds from aromatic units that have condensed into larger sheets during pyrolysis (Huang *et al.* 2018, Li *et al.* 2019, Bandara *et al.* 2020). All three biochar samples showed similar identified peaks.

According to the literature, heavy metal adsorption to biochar is positively correlated with the surface functional groups containing oxygen and the amorphous regions (Inyang *et al.* 2016, Shaheen *et al.* 2019, Duan *et al.* 2020, Wang *et al.* 2020, Sharma *et al.* 2022). In order to differentiate the effect of various biochar samples, the oxygen-containing functional groups and the amorphous regions were quantitatively characterized using FT-IR spectra. The peak area ratios of 1697 cm^{-1} (C = O) and 1435 cm^{-1} (C–H stretching) relative to the peak at 1582 cm^{-1} (aromatic C = C stretching) (i.e. $I_{C=O}/I_{C=C}$ and $I_{C-H}/I_{C=C}$) were calculated, and the data are shown in Table 3. The peak areas were calculated using the peak area function of the Spectrum 6 Spectroscopy Software (PerkinElmer, Waltham, MA, USA). The areas for the C = O, C = C, and C–H peaks were calculated in the wavenumber ranges of 1720 – 1670, 1655 – 1486, and 1486 – 1365 cm^{-1}. The statistical analysis of the peak area ratios for the three biochar samples (L15-0M, L30-0M, and L39-0M) indicated that the C = O to C = C ratios for L15-0M and L39-0M are significantly higher than that of L30-0M. For the peak area ratios of C–H to C = C, similar trends were observed, while statistical analysis showed that there is no significant difference among the three biochar samples.

The effect of the environmental exposure period of the wood samples on the biochar functional groups was also investigated using FT-IR. For the biochar samples manufactured from wood with 6 and 12 months of environmental exposure, FT-IR spectra (not shown in this study) with the same peaks were observed compared with those having 0 months of environmental exposure period within the same tree maturity group. The same area ratios from the FT-IR spectra were calculated, as shown in Table 3. The statistical analysis showed that the biochar sample L15-12M has a lower peak area ratio for C = O to C = C than those of L15-0M and L15-6M. For the biochar samples manufactured from the wood samples at 30 and 39 years old, there is no difference in the peak area ratios of C = O to C = C. For the peak area ratios of C–H to C = C, there is no significant difference for the biochar samples produced from 15- and 39-year-old wood samples with the three different environmental exposure periods. For the biochar manufactured from the 30-year-old tree, the 6 months of environmental exposure to the wood produced a biochar sample with a higher peak area ratio of C–H to C = C than those with 0 and 12 months of environmental exposure periods. The quantitative analysis of the FT-IR spectra showed biochar samples made from wood at different tree maturities have the same functional groups with different ratios of the same functional groups. The environmental exposure to wood didn't impact the functional groups of biochar in a specific pattern. A random change of the biochar functional group ratios was observed for a specific sample of L15-12M and L30-6M.

Raman spectroscopy was used to probe the carbon-based biochar structure for all the samples. Raman spectroscopy has been widely used to characterize the structure of carbon-based material due to its advantages of easy sample preparation, high sensitivity, high resolution, and non-destructive nature (Potgieter-Vermaak *et al.* 2011, Smith *et al.* 2016, Guizani *et al.* 2017). Studies on biochar carbon structure change and evolution during the pyrolysis process of biomass have been performed using Raman spectroscopy (Tsaneva *et al.* 2014, Smith *et al.* 2016, Guizani *et al.* 2017, Yu *et al.* 2018). In this study, Raman spectroscopy was employed to assess the carbon-based structure change impacted by the feedstock tree maturity and environmental exposure period. In the Raman spectra of biochar samples, two characteristic bands located at about 1342 (D band) and 1581(G band) cm^{-1} were observed, and the ratio of the D/G band was used to characterize the structure change of the biochar samples. The D band is known as the disorder band of the graphite structure originating in structural defects or edge effects (Adar 2022). The G band is due to the in-plane stretching motion between sp^2 carbon atoms and represents the planar configuration of sp^2 bonded carbon in graphene and graphite structure (Yu *et al.* 2018). The change in the ratio of D/G indicates the biochar structure change toward more disordered. The Raman spectra for the biochar samples of L15-0M, L30-0M,

Table 3. The quantitative analysis of the biochar functional groups.

	$I_{C=O}/I_{C=C}$			$I_{C-H}/I_{C=C}$		
Sample	0M	6M	12M	0M	6M	12M
L15	0.053±0.003	0.067±0.003	0.040±0.006	0.32±0.01	0.31±0.02	0.34±0.05
L30	0.033±0.003	0.040±0.000	0.040±0.000	0.25±0.02	0.34±0.04	0.23±0.01
L39	0.060±0.006	0.043±0.003	0.050±0.000	0.31±0.01	0.28±0.01	0.23±0.01

and L39-0M are shown in Figure 3. The D/G ratios for all the samples are also shown as an insert in Figure 3. Statistical analysis showed that all the biochar samples have no significant difference in D/G ratios, indicating that the tree maturity and environmental exposure didn't significantly change the carbon-based structure for all the biochar samples.

Biochar pH and EC

Biochar pH values are important given their influence on other properties and various applications, such as heavy metal adsorption and soil amendment. From the literature, biochar pH values between 3.1 and 12.0 have been reported (Lehmann 2007, Mukherjee *et al.* 2011). The pH values of biochar samples are correlated with the formation of carbonates and the contents of inorganic alkalis which are associated with the feedstocks and the manufacturing processes (Tomczyk *et al.* 2020). In this study, the pH values of all the biochar samples measured are shown in Table 2, and the pH values ranged from 4.71±0.01 to 6.03±0.01. The acidity of the biochar samples is mainly caused by the low pyrolysis temperature for loblolly pine trees at 450 °C, and the results are consistent with the literature data (Stefanko and Leszczynska 2020). The statistical analysis indicated that both tree maturity and environmental exposure period impact the pH values of the biochar samples. There is a significant difference in pH values for biochar samples of L15-0M, L30-0M, and L39-0M, with values of 5.26 ± 0.01, 6.03 ± 0.01, and 5.52 ± 0.01, respectively. The L30-0M biochar sample has a much higher pH value than the other two, which correlated well with the FT-IR results with a lower C = O to C = C ratio shown in Table 3. After 6 and 12 months of environmental exposure, the pH of the biochar samples made from a 15-year-old tree increased from 5.26 ± 0.01 to 5.37 ± 0.01 and 5.41 ± 0.06, respectively. For the biochar samples made from 30- and 39-year-old trees, the pH values didn't change for 6 months of environmental exposure to wood, while they significantly decreased with 12 months of environmental exposure (Table 4). The lowest biochar pH value was observed to be 4.71 ± 0.01 with the sample of L39-12M. Both the tree maturity and environmental exposure significantly changed the biochar pH values.

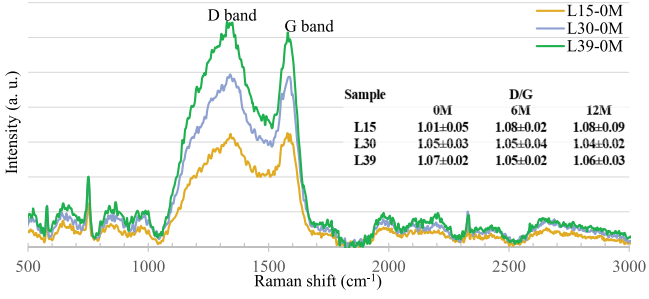

Figure 3. The Raman spectra of the biochar samples of L15-0M, L30-0M, and L39-0M.

The EC values for all the biochar samples are also shown in Table 4. The EC was measured in biochar solution based on the principle that solutions with a higher concentration of dissolved salts have a greater ability to conduct an electrical current, and the EC is proportional to the quantity and nature of salts dissolved in the solution. Understanding the amount of soluble salts in a biochar solution is important when considering heavy metal (Pb^{2+}) adsorption in aqueous solutions. From reviewing the literature, the EC of biochar ranges from 0.04 to 54.2 dS/m, mainly determined by the feedstock and manufacturing temperature (Singh *et al.* 2010, Cantrell *et al.* 2012, Rajkovich *et al.* 2012, Claoston *et al.* 2014, Rehrah *et al.* 2014, Smider and Singh 2014). Biochar manufactured from feedstock with higher ash content and higher pyrolysis temperature generally has higher EC (Cantrell *et al.* 2012, Claoston *et al.* 2014, Rehrah *et al.* 2014, Smider and Singh 2014). In this study, the EC values are in the range of 0.10 ± 0.02 – 0.30 ± 0.01 dS/m (Table 4). For the biochar samples made from three different ages of trees, L15-0M has a higher EC than the other two, mainly caused by the higher ash content as measured in our previous publication (Peng *et al.* 2024). No significant difference in EC was observed for biochar samples between L30-0M and L39-0M. For the biochar made from the same age of the tree, the EC changes vary with the environmental exposure period. The EC of biochar L15-12M (0.14 ± 0.02) is significantly lower than those of L15-0M (0.22 ± 0.01) and L15-6M (0.27 ± 0.08), which do not differ significantly from each other. For the biochar made from the 30-year-old tree, the L30-6M has greater EC than the other two. For the biochar samples from the 39-year-old tree, all have different ECs, with the greatest EC of 0.30 ± 0.01 dS/m for the L39-6M. These EC changes for the biochar samples didn't match the changes in the ash contents for all the wood samples (Peng *et al.* 2024), even with the same pyrolysis procedures. These observations indicated that other factors, including wood degradation due to exposure to the environment, may significantly change the biochar formation mechanisms during the pyrolysis process.

Biochar SSA

The CO_2 adsorption on biochar was carried out at 0 °C, and the obtained adsorption isotherms for biochar samples of L15-0M, L30-0M, and L39-0M are presented in Figure 4a. The Dubinin-Astakhov equation provided a linear line to fit the CO_2 isotherms, as shown in Figure 4b. The parameters based on the Dubinin-Astakhov equation for all the biochar samples are summarized in Table 5. The Astakhov exponent (n) values for all the biochar samples are greater than 2, and the

Table 4. The pH and EC of all the biochar samples.

	pH			EC (dS/m)		
Sample	0M	6M	12M	0M	6M	12M
L15	5.26±0.01	5.37±0.01	5.41±0.06	0.22±0.01	0.27±0.08	0.14±0.02
L30	6.03±0.01	6.01±0.01	5.24±0.01	0.10±0.02	0.18±0.01	0.12±0.01
L39	5.52±0.01	5.51±0.01	4.71±0.01	0.15±0.02	0.30±0.01	0.24±0.02

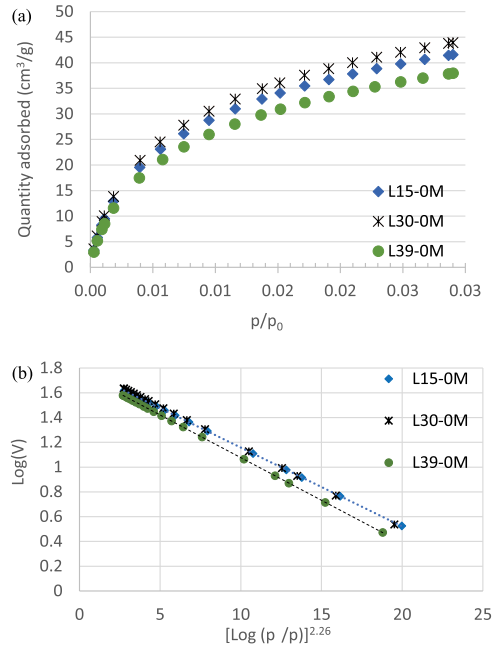

Figure 4. The CO_2 adsorption isotherms of the biochar samples and the Dubinin-Astakhov equation fitting.

characteristic energy (E_0) numbers are all approximately 17.5 kJ/mol. The Dubinin-Astakhov equation was established based on a model in which the adsorption is associated with the adsorbent site energies (Dubinin and Stoeckli 1980). The Astakhov exponent reflects the distribution of the energy sites, which is related to the pore size distribution of the adsorbents. The Astakhov exponent values between 1 and 4 have been obtained for most carbon-based adsorbents, and a value greater than 2 indicates a homogeneous carbon adsorbent with most of the pores in the micropore range (Finger and Bulow 1979, Hu and Ruckenstein 2006). The values of the Astakhov exponent for all the biochar samples are around 2.3, which indicates that the biochar samples produced in this study are homogeneous microporous carbon. No significant difference was observed for the Astakhov exponent for biochar samples made from different tree maturities and environmental exposure periods. The same case for the characteristic energy was observed (Table 4). The derived SSA of all the biochar samples are included in Table 4. The SSA values for the L15-0M, L30-0M, and L39-0M are 313 ± 10, 338, and 293 ± 9 m^2/g, respectively, based on the measurement of two replicates. The L30-0M has a higher SSA than that of L15-0M, which is greater than that of L39-0M. For the biochar samples made from the same tree maturity, the environmental exposure of the wood changed the SSA. No pattern was observed for the change, though. After 12 months of environmental exposure to the 15-year-old tree, the biochar manufactured increased the SSA from 313 ± 10 to 337 ± 2 m^2/g. For the biochar made from the 30-year-old tree, the environmental exposure of the wood for 6 and 12 months decreased slightly the SSA from 338 m^2/g to 326 ± 4 and 329 ± 2 m^2/g, respectively. Similarly, 12 months of environmental exposure to the 39-year-old tree decreased the biochar SSA from 293 ± 9 to 278 ± 2 m^2/g. Therefore, the environmental exposure to the wood resulted in mixed results of the biochar SSA changes. The biochar sample made from the 39-year-old tree with 12 months of environmental exposure has the lowest SSA of 278 2 m^2/g.

Biochar lead ion adsorption isotherm

The calibration curve used to measure the Pb^{2+} concentration in solutions is shown in Figure 5a, with the ion concentration range of 1 – 30 mg/L. After applying the biochar in Pb^{2+} solution for 72 h, the concentrations of ions in solutions (C_e) were measured to calculate the quantity of ions adsorbed by the biochar sample. The amount of adsorption on biochar at equilibrium can be obtained (q_e), and the Pb^{2+} adsorption isotherms were then plotted as q_e versus Ce. The representative adsorption isotherms for the biochar samples of L15-0M, L30-0M, and L39-12M are shown in Figure 5b. The biochar sample of L39-12M is included to show the significant differences in Pb^{2+} adsorption capacities among biochar samples. The establishment of the linear relationship using equation 3 was performed for (C_e/q_e) against C_e, and the corresponding linear relationships for the biochar samples of L15-0M, L30-0M, and L39-12M are shown in Figure 5c. The Langmuir models used to fit the isotherm data are shown in Figure 5d. The maximum adsorption capacity (qm) and Langmuir isotherm constant (K_L) can then be calculated from the linear relationship. The q_m and K_L values for all the biochar samples are shown in Table 6.

For the biochar samples made from wood with three different maturities, the Pb^{2+} adsorption capacities are 4.02 ±0.06, 2.91±0.16, and 2.55±0.06 mg/g for L15-0M, L30-0M, and L39-0M, respectively, and the statistical analysis indicated that the adsorption capacities are significantly different. The tree maturity impacts the biochar samples' adsorption capacity of Pb^{2+}. The Pb^{2+} adsorption capacities of the biochar samples were qualitatively correlated with different physicochemical properties of the samples. It seems that the biochar pH, EC, SSA, and surface functional groups are all involved, and no single factor can be used to explain the higher Pb^{2+} adsorption capacity of L15-0M than those of L30-0M and L39-0M. The lower pH (5.26) and higher EC (0.22 dS/m) of the L15-0M sample than those of L30-0M (6.03 and 0.1 dS/m, respectively) can explain the higher Pb^{2+} adsorption capacity of L15-0M. Simultaneously, the surface functional groups of L15-0M have

Table 5. The Dubinin-Astakhov parameters for CO_2 adsorption by biochar samples and the derived specific surface areas.

	n			E_0 (kJ/mol)			SSA (m^2/g)		
Sample	0M	6M	12M	0M	6M	12M	0M	6M	12M
L15	2.34±0.02	2.33±0.00	2.37±0.00	17.5±0.0	17.5±0.0	17.5±0.0	313±10	318±7	337±2
L30	2.36±0.02	2.35±0.01	2.35±0.01	17.5±0.1	17.5±0.1	17.5±0.0	338±0	326±4	329±2
L39	2.31±0.00	2.32±0.01	2.32±0.01	17.4±0.1	17.5±0.1	17.4±0.0	293±9	305±12	278±2

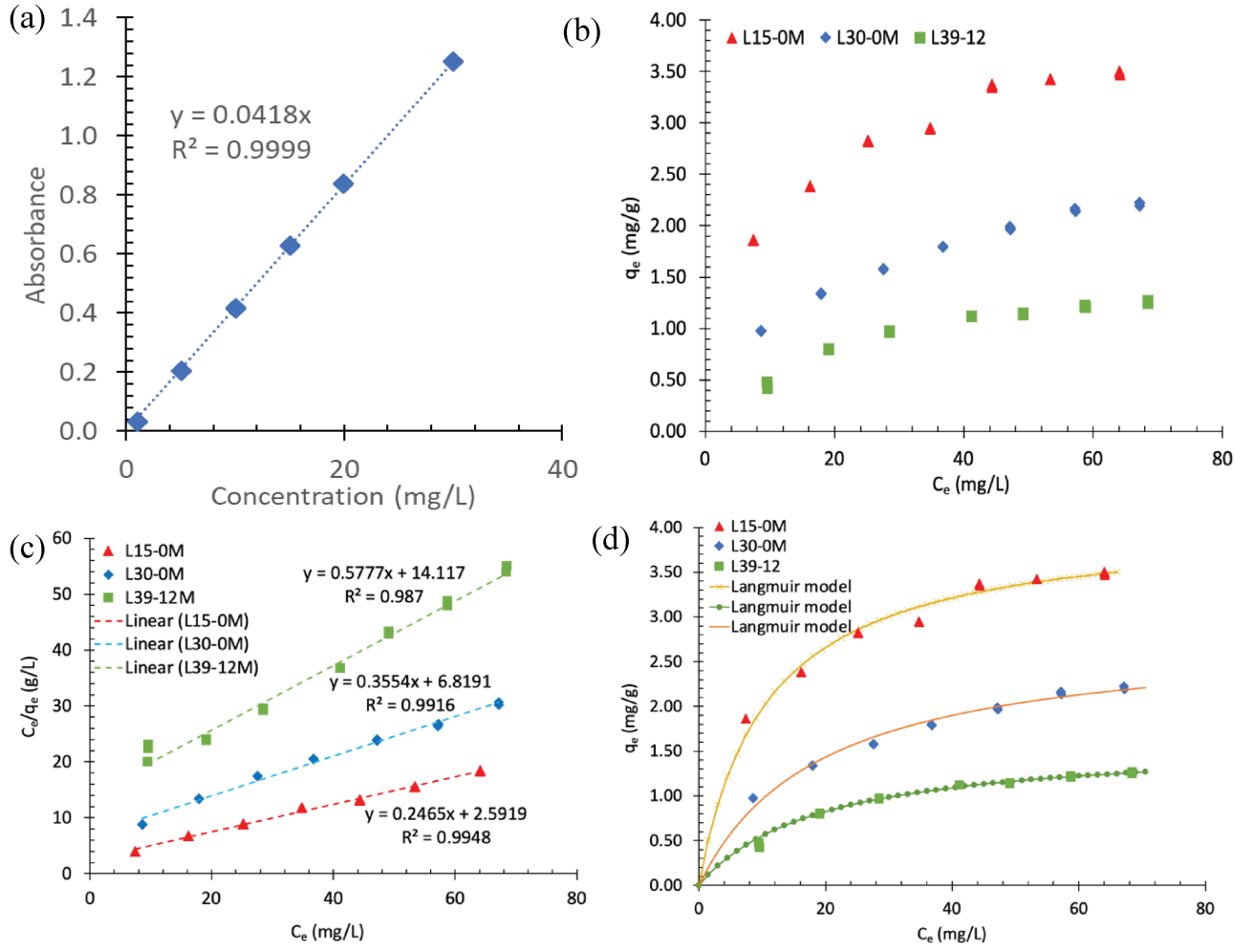

Figure 5. The calibration curve for measuring Pb^{2+} in solutions using a UV/Vis spectrophotometer (a) and the representative Pb^{2+} adsorption isotherms of biochar samples (b), the linear relationship using the Langmuir model to fit the adsorption isotherm data (c) and the isotherm data fitted with Langmuir models for the biochar samples (d).

Table 6. The predicted Pb^{2+} adsorption capacity using the Langmuir model and the Langmuir constants for all the biochar samples.

	q_m (mg/g)			K_L (L/mg)		
Sample	0M	6M	12M	0M	6M	12M
L15	4.02±0.06	4.09±0.20	3.14±0.05	0.095±0.008	0.1172±0.042	0.0500±0.010
L30	2.91±0.16	3.39±0.02	2.97±0.27	0.037±0.015	0.1787±0.028	0.2613±0.016
L39	2.55±0.06	4.78±0.15	1.59±0.05	0.0418±0.007	0.0845±0.007	0.0568±0.005

a much greater $I_{C=O}$ to $I_{C=C}$ ratio (Table 3), which can also contribute to the lower pH and higher Pb^{2+} adsorption capacity. However, this theory cannot explain the higher Pb^{2+} adsorption capacity of L30-0M over that of L39-0M. The biochar of L39-0M has a lower pH (5.52) and higher EC (0.15) than that of L30-0M. The L39-0M also has a greater $I_{C=O}$ to $I_{C=C}$ ratio than that of L30-0M. At this point, the SSA of the biochar samples needs to be considered. The biochar sample of L30-0M has a much higher SSA (338 m^2/g) when compared with the biochar sample of L39-0M (293 m^2/g). Therefore, all the factors, including pH, EC, surface functional group, and SSA played a role in determining the Pb^{2+} adsorption capacity. The effect of each factor on the Pb^{2+} adsorption capacity may need to be considered for each specific case. The Langmuir constants (K_L) for the biochar samples are also shown in Table 6. A larger number of the Langmuir constant indicates a stronger binding property between the Pb^{2+} and the biochar surface. The biochar of L15-0M has a much greater K_L value than the other two biochar samples, which are of the same magnitude. The stronger interaction between Pb^{2+} and the biochar of L15-0M may also contribute to the higher adsorption capacity compared with the other two biochar samples.

For the biochar samples made from wood with the same tree maturity, the effect of the environmental exposure period on Pb^{2+} adsorption capacity differs with the age of the wood. For the three biochar samples of L15-0M, L15-6M, and L15-12M, the Pb^{2+} adsorption capacities are 4.02±0.06, 4.09±0.20, and 3.14±0.05 mg/g. After 12 months of

environmental exposure, the Pb^{2+} adsorption capacity of the biochar decreased significantly (22%), while 6 months of environmental exposure to the wood did not change the biochar Pb^{2+} adsorption capacity. For the biochar samples made from the 30-year-old tree, 6 months of environmental exposure significantly increased the Pb^{2+} adsorption capacity (3.39±0.02 mg/g) when compared to the biochar samples of L30-0M (2.91±0.16) and L30-12M (2.97±0.27 mg/g). The biochar samples manufactured from the 39-year-old tree behaved differently when compared with the samples from the 15- and 30-year-old trees. The environmental exposure of 6 months significantly increased the biochar performance in Pb^{2+} adsorption capacity from 2.55±0.06 mg/g to 4.78±0.15 mg/g, an 87% increase. The 12 months of environmental exposure to the wood decreased the biochar Pb^{2+} adsorption capacity to 1.59±0.05 mg/g, a 67% reduction compared with that of L39-6M. The effect of environmental exposure to the wood changed the Pb^{2+} adsorption capacities of the biochar samples, and the impacts are different for different ages of trees. However, 6 months of environmental exposure to the wood significantly enhanced the biochar performance in Pb^{2+} adsorption capacity, while 12 months of environmental exposure significantly decreased the Pb^{2+} adsorption capacity. The biochar sample of L39-6M has the greatest adsorption capacity for Pb^{2+}, and the sample of L39-12M has the lowest. The lowest Pb^{2+} adsorption capacity of L39-12M is correlated well with the lowest pH and SSA of this biochar sample. The other factors, including the EC and surface functional group, may also contribute to the Pb^{2+} adsorption capacity. There is no single physicochemical property that dominates the effect on the biochar's capability to adsorb the Pb^{2+} in this study.

The change in the Langmuir constants can also be observed. The environmental exposure of the wood for 6 months increased the Langmuir constant values (Table 6), indicating that the binding energy between the Pb^{2+} and biochar surface became stronger. The environmental exposure of 12 months decreased the binding energy between Pb^{2+} and biochar surface for the biochar samples of L15-12M and L39-12M. However, the binding between Pb^{2+} and the biochar surface increased for the biochar sample of L30-12M when compared with that of L30-6M. Therefore, the environmental exposure of wood changed the surface properties of biochar manufactured using the pyrolysis process and the effects varied with different maturities of the wood sample.

Conclusions

Loblolly pine samples with different tree ages and environmental exposure periods to the southeastern US weather conditions were used to manufacture biochar samples using a pyrolysis process under N_2 at 450 °C. The environmental exposure periods of 0, 6, and 12 months were employed to collect the log samples with tree maturities of 15-, 30-, and 39-year-olds. The research hypothesis is that the biochar samples manufactured from downed timber with different maturities and environmental exposure periods behave differently in adsorbing lead ions, and the differences are correlated with the physicochemical characteristics. The biochar samples were characterized for their physicochemical properties, including morphologies, elemental compositions, surface functional groups, carbon structure, pH, EC, and surface area. The Pb^{2+} adsorption isotherms were also measured for all the biochar samples.

The morphologies characterization of the biochar showed that the microstructures of wood were largely maintained after pyrolysis. No obvious difference was observed in morphologies for the biochar samples made from wood samples with different tree maturities and environmental exposure periods. No significant differences were observed for elemental compositions and carbon structures. The carbon, hydrogen, and oxygen contents for all the biochar samples ranged from 82.0 – 85.3, 3.5 – 3.8, and 10.9 – 14.6%. The pH and EC values showed significant differences and were impacted by the tree maturities and the environmental exposure periods. The biochar generated from 30-year-old wood has a higher pH of 6.03 than that from 39-year-old wood (5.52), followed by the lowest pH biochar from 15-year-old wood (5.26). The environmental exposure of the wood for 6 months did not change the pH of the biochar samples, while 12 months of environmental exposure caused a significant change in the biochar pH. The SSAs of biochar samples are also different due to the different tree maturities and environmental exposure periods. The biochar produced from the 39-year-old tree with 12 months of exposure to the environment has the lowest SSA of 278 ± 2 m^2/g. The Pb^{2+} adsorption capacities of all the biochar samples were significantly impacted by the tree maturities and the environmental exposure periods. The Pb^{2+} adsorption capacities of the biochar samples are in the order: L15-0M (4.02 ± 0.06 mg/g) > L39-0M (2.91 ± 0.16 mg/g) > L39-0M (2.55 ± 0.06 mg/g). The environmental exposure period of 6 months significantly increased the Pb^{2+} adsorption capacities for all the biochar samples, and the 12-month environmental exposure period significantly decreased the Pb^{2+} adsorption capacity for all the biochar samples.

The research hypothesis has been confirmed that the lead ion adsorption capacities of biochar samples are different, and the physicochemical characteristics of biochar, especially pH, EC, and SSA, significantly affect the lead ion adsorption capacities. An effort was made to correlate the biochar Pb^{2+} adsorption capacity and the biochar physicochemical properties, and the results indicated that there is an interaction among the physicochemical properties of the biochar samples that dominates the effect on Pb^{2+} adsorption capacity. For each specific biochar system for a specific heavy metal mitigation in wastewater, a case-by-case study in the laboratory is suggested to be performed before the field trials. Future work should focus on further understanding the relationship between biochar physicochemical properties and heavy metal adsorption capacities in greater depth. The research results also indicated that the downed timber collected at different times impacts the biochar physicochemical characteristics and its behaviors in adsorbing lead ions, offering valuable information for biochar manufacturing industries.

Data availability statement

The data that support the findings of this study are available from the corresponding author, [YP], upon reasonable request.

Disclosure statement

No potential conflict of interest was reported by the author(s).

Funding

This work was supported by the U.S. Endowment for Forestry & Communities [grant no G00016056]; USDA Forest Service [grant no 24-JV-11330101-004]; Southern Research Station [grant no 23-JV-11330170-064].

References

Abdullaev, S.S., et al., 2023. Study of the kinetic, equilibrium, and thermodynamic aspects of the removal and recovery of divalent lead heavy metal ions from industrial wastewaters contaminated by vesavin-enriched XAD-11600 amberlite resin. *Heliyon*, 9, doi:10.1016/j.heliyon.2023.e22761.

Adar, F., 2022. Use of Raman spectroscopy to qualify carbon materials. *Spectroscopy-Us*, 37, 11–15.

Bandara, T., et al., 2020. Mechanisms for the removal of Cd(II) and Cu(II) from aqueous solution and mine water by biochars derived from agricultural wastes. *Chemosphere*, 254, doi:10.1016/j.chemosphere.2020.126745.

Bansal, R.C., and Goyal, M., 2005. *Activated carbon adsorption*. Boca Raton, FL: CRC Press.

Cantrell, K.B., et al., 2012. Impact of pyrolysis temperature and manure source on physicochemical characteristics of biochar. *Bioresource Technology*, 107, 419–428. doi:10.1016/j.biortech.2011.11.084.

Carolin, C.F., et al., 2017. Efficient techniques for the removal of toxic heavy metals from aquatic environment: A review. *Journal of Environmental Chemical Engineering*, 5, 2782–2799. doi:10.1016/j.jece.2017.05.029.

Carrascomarin, F., Lopezramon, M.V., and Morenocastilla, C., 1993. Applicability of the dubinin radushkevich equation to Co2 adsorption on activated carbons. *Langmuir*, 9, 2758–2760. doi:10.1021/la00035a002.

Chai, W.S., et al., 2021. A review on conventional and novel materials towards heavy metal adsorption in wastewater treatment application. *Journal of Cleaner Production*, 296, doi:10.1016/j.jclepro.2021.126589.

Chen, X.Y., et al., 2022. Isotherm models for adsorption of heavy metals from water-A review. *Chemosphere*, 307, doi:10.1016/j.chemosphere.2022.135545.

Chen, S.G., and Yang, R.T., 1994. Theoretical basis for the potential-theory adsorption-isotherms - the dubinin-radushkevich and dubinin-astakhov equations. *Langmuir*, 10, 4244–4249. doi:10.1021/la00023a054.

Claoston, N., et al., 2014. Effects of pyrolysis temperature on the physicochemical properties of empty fruit bunch and rice husk biochars. *Waste Management & Research: The Journal for a Sustainable Circular Economy*, 32, 331–339. doi:10.1177/0734242x14525822.

Collard, F.X., and Blin, J., 2014. A review on pyrolysis of biomass constituents: mechanisms and composition of the products obtained from the conversion of cellulose, hemicelluloses and lignin. *Renewable and Sustainable Energy Reviews*, 38, 594–608. doi:10.1016/j.rser.2014.06.013.

Duan, C.Y., et al., 2020. Removal of heavy metals from aqueous solution using carbon-based adsorbents: A review. *Journal of Water Process Engineering*, 37, doi:10.1016/j.jwpe.2020.101339.

Dubinin, M.M., and Stoeckli, H.F., 1980. Homogeneous and heterogeneous micropore structures in carbonaceous adsorbents. *Journal of Colloid and Interface Science*, 75, 34–42. doi:10.1016/0021-9797(80)90346-X.

Finger, G., and Bulow, M., 1979. Applicability of the dubinin-astakhov equation in the sorption systems normal-heptane-saran carbon and benzene-saran carbon. *Carbon*, 17, 7–91. doi:10.1016/0008-6223(79)90074-5.

Freschet, G.T., et al., 2013. Linking litter decomposition of above- and below-ground organs to plant-soil feedbacks worldwide. *Journal of Ecology*, 101, 943–952. doi:10.1111/1365-2745.12092.

Fu, F.L., and Wang, Q., 2011. Removal of heavy metal ions from wastewaters: A review. *Journal of Environmental Management*, 92, 407–418. doi:10.1016/j.jenvman.2010.11.011.

Gautam, R.K., et al., (2015) Contamination of heavy metals in aquatic media: transport, toxicity and technologies for remediation. In *Heavy Metals in Water: Presence, Removal and Safety*ECCC Environmental eBooks 1968-2022, pp. 1–24.

Goodell, B., Winandy, J.E., and Morrell, J.J., 2020. Fungal degradation of wood: emerging data, New insights and changing perceptions. *Coatings*, 10, doi:10.3390/coatings10121210.

Guizani, C., et al., 2017. New insights on the structural evolution of biomass char upon pyrolysis as revealed by the Raman spectroscopy and elemental analysis. *Carbon*, 119, 519–521. doi:10.1016/j.carbon.2017.04.078.

Han, Y.X., et al., 2013. Heavy metal and phenol adsorptive properties of biochars from pyrolyzed switchgrass and woody biomass in correlation with surface properties. *Journal of Environmental Management*, 118, 196–204. doi:10.1016/j.jenvman.2013.01.001.

Hu, Y.H., and Ruckenstein, E., 2006. Applicability of Dubinin-Astakhov equation to CO_2 adsorption on single-walled carbon nanotubes. *Chemical Physics Letters*, 425, 306–310. doi:10.1016/j.cplett.2006.05.059.

Huang, F., et al., 2018. Quantitative contribution of Cd^{2+} adsorption mechanisms by chicken-manure-derived biochars. *Environmental Science and Pollution Research*, 25, 28322–28334. doi:10.1007/s11356-018-2889-y.

Hutson, N.D., and Yang, R.T., 1997. Theoretical basis for the Dubinin-Radushkevitch (D-R) adsorption isotherm equation. *Adsorption*, 3, 189–195. doi:10.1007/Bf01650130.

Inyang, M.I., et al., 2016. A review of biochar as a low-cost adsorbent for aqueous heavy metal removal. *Critical Reviews in Environmental Science and Technology*, 46, 406–433. doi:10.1080/10643389.2015.1096880.

Krah, F.S., et al., 2018. Evolutionary dynamics of host specialization in wood-decay fungi. *BMC Evolutionary Biology*, 18, doi:10.1186/s12862-018-1229-7.

Kurniawan, T.A., et al., 2006. Physico-chemical treatment techniques for wastewater laden with heavy metals. *Chemical Engineering Journal*, 118, 83–98. doi:10.1016/j.cej.2006.01.015.

Larson PR, Kretschmann DE, Clark A, Isebrands JG (2001) Formation and properties of juvenile wood in southern pines. Madison, WI: USDA Forest Service Forest Products Laboratory

Lehmann, J., 2007. Bio-energy in the black. *Frontiers in Ecology and the Environment*, 5, 381–387. doi:10.1890/1540-9295(2007)5[381:Bitb]2.0.Co;2.

Li, L.C., et al., 2019. Biochar as a sorbent for emerging contaminants enables improvements in waste management and sustainable resource use. *Journal of Cleaner Production*, 210, 1324–1342. doi:10.1016/j.jclepro.2018.11.087.

Lu, C.Q., et al., 2021. Influence of juvenile and mature wood on anatomical and chemical properties of early and late wood from Chinese fir plantation. *Journal of Wood Science*, 67, doi:10.1186/s10086-021-02005-2.

Mahmoud, S.H., Gan, T.Y., and Zhu, D.Z., 2023. Impacts of climate change and climate variability on water resources and drought in an arid region and possible resiliency and adaptation measures against climate warming. *Climate Dynamics*, 61, 4079–4105. doi:10.1007/s00382-023-06795-7.

Marousek, J., and Trakal, L., 2022. Techno-economic analysis reveals the untapped potential of wood biochar. *Chemosphere*, 291, doi:10.1016/j.chemosphere.2021.133000.

Mukherjee, A., Zimmerman, A.R., and Harris, W., 2011. Surface chemistry variations among a series of laboratory-produced biochars. *Geoderma*, 163, 247–255. doi:10.1016/j.geoderma.2011.04.021.

Mukome, F.N.D., Six, J., and Parikh, S.J., 2013. The effects of walnut shell and wood feedstock biochar amendments on greenhouse gas emissions from a fertile soil. *Geoderma*, 200, 90–98. doi:10.1016/j.geoderma.2013.02.004.

Olsen, J.R., Dettinger, M.D., and Giovannettone, J.P., 2023. Drought attribution studies and water resources management. *Bulletin of the American Meteorological Society*, 104, E435–E441. doi:10.1175/Bams-D-22-0214.1.

Oswalt, S.N., et al., 2019. *Forest resources of the United States, 2017: a technical document supporting the forest service 2020 RPA assessment*. Washington, DC: U.S. Department of Agriculture, Forest Service. doi:10.2737/WO-GTR-97.

Peng, Y.C., et al., 2024. Wood fiber production from downed timber for manufacturing wood polymer composite: fiber property characterization. *Wood Material Science & Engineering*, 19, 541–555. doi:10.1080/17480272.2023.2266832.

Potgieter-Vermaak, S., et al., 2011. Raman spectroscopy for the analysis of coal: a review. *Journal of Raman Spectroscopy*, 42, 123–129. doi:10.1002/jrs.2636.

Qasem, N.A.A., Mohammed, R.H., and Lawal, D.U., 2021. Removal of heavy metal ions from wastewater: a comprehensive and critical review. *Npj Clean Water*, 4, doi:10.1038/s41545-021-00127-0.

Rajkovich, S., et al., 2012. Corn growth and nitrogen nutrition after additions of biochars with varying properties to a temperate soil. *Biology and Fertility of Soils*, 48, 271–284. doi:10.1007/s00374-011-0624-7.

Rayner, A.D.M., and Boddy, L., 1988. *Fungal decomposition of wood, its biology and ecology*. Chichester: Wiley.

Rehrah, D., et al., 2014. Production and characterization of biochars from agricultural by-products for use in soil quality enhancement. *Journal of Analytical and Applied Pyrolysis*, 108, 301–309. doi:10.1016/j.jaap.2014.03.008.

Schoennagel, T., Veblen, T.T., and Romme, W.H., 2004. The interaction of fire, fuels, and climate across rocky mountain forests. *Bioscience*, 54, 661–676. doi:10.1641/0006-3568(2004)054[0661:Tioffa]2.0.Co;2.

Shaheen, S.M., et al., 2019. Wood-based biochar for the removal of potentially toxic elements in water and wastewater: a critical review. *International Materials Reviews*, 64, 216–247. doi:10.1080/09506608.2018.1473096.

Sharma, A., Anjana, R.H., and Goswami, S., 2022. A comprehensive review on the heavy metal removal for water remediation by the application of lignocellulosic biomass-derived nanocellulose. *Journal of Polymers and the Environment*, 30, 1–18. doi:10.1007/s10924-021-02185-4.

Shin, S.M., Park, J.K., and Jung, S.M., 2015. Changes of aromatic CH and aliphatic CH in In-situ FT-IR spectra of bituminous coals in the thermoplastic range. *ISIJ International*, 55, 1591–1598. doi:10.2355/isijinternational.ISIJINT-2014-625.

Shmulsky, R., and Jones, P.D., 2019. *Forest products and wood science: an introduction*. Hoboken, NJ: Wiley-Blackwell.

Singh, B., et al. (2017) Biochar pH, electrical conductivity and liming potential. In *Biochar: A Guide to Analytical Methods*. Boca Raton, FL: CRC Press, pp. 23–38.

Singh, B., Singh, B.P., and Cowie, A.L., 2010. Characterisation and evaluation of biochars for their application as a soil amendment. *Soil Research*, 48, 516–525. doi:10.1071/Sr10058.

Smider, B., and Singh, B., 2014. Agronomic performance of a high ash biochar in two contrasting soils. *Agriculture, Ecosystems & Environment*, 191, 99–107. doi:10.1016/j.agee.2014.01.024.

Smith, M.W., et al., 2016. Structural analysis of char by Raman spectroscopy: improving band assignments through computational calculations from first principles. *Carbon*, 100, 678–692. doi:10.1016/j.carbon.2016.01.031.

Stefanko, A.U., and Leszczynska, D., 2020. Impact of biomass source and pyrolysis parameters on physicochemical properties of biochar manufactured for innovative applications. *Frontiers in Energy Research*, 8, doi:10.3389/fenrg.2020.00138.

Stewart, C., et al., 2006. Contamination of water supplies by volcanic ashfall: A literature review and simple impact modelling. *Journal of Volcanology and Geothermal Research*, 158, 296–306. doi:10.1016/j.jvolgeores.2006.07.002.

Svoboda, M., et al., 2010. Natural development and regeneration of a central European montane spruce forest. *Forest Ecology and Management*, 260, 707–714. doi:10.1016/j.foreco.2010.05.027.

Tomczyk, A., Sokolowska, Z., and Boguta, P., 2020. Biochar physicochemical properties: pyrolysis temperature and feedstock kind effects. *Reviews in Environmental Science and Bio/Technology*, 19, 191–215. doi:10.1007/s11157-020-09523-3.

Tsaneva, V.N., et al., 2014. Assessment of the structural evolution of carbons from microwave plasma natural gas reforming and biomass pyrolysis using Raman spectroscopy. *Carbon*, 80, 617–628. doi:10.1016/j.carbon.2014.09.005.

Uprety, S., et al., 2017. The effect of the 2015 earthquake on the bacterial community compositions in water in Nepal. *Frontiers in Microbiology*, 8, doi:10.3389/fmicb.2017.02380.

Vardhan, K.H., Kumar, P.S., and Panda, R.C., 2019. A review on heavy metal pollution, toxicity and remedial measures: current trends and future perspectives. *Journal of Molecular Liquids*, 290, doi:10.1016/j.molliq.2019.111197.

Villarín, M.C., and Merel, S., 2020. Paradigm shifts and current challenges in wastewater management. *Journal of Hazardous Materials*, 390, doi:10.1016/j.jhazmat.2020.122139.

Wang, X.Q., et al., 2020. Recent advances in biochar application for water and wastewater treatment: a review. *Peerj*, 8, doi:10.7717/peerj.9164.

Wang, L., et al., 2022. Fast pyrolysis of guaiacyl-syringyl (GS) type milled wood lignin: product characteristics and CH4 formation mechanism study. *Science of The Total Environment*, 838, doi:10.1016/j.scitotenv.2022.156395.

Weaver, J.K., et al., 2009. Decaying wood and tree regeneration in the acadian forest of Maine, USA. *Forest Ecology and Management*, 257, 1623–1628. doi:10.1016/j.foreco.2009.01.023.

Woodall, C.W., et al., 2013. Biomass and carbon attributes of downed woody materials in forests of the United States. *Forest Ecology and Management*, 305, 48–59. doi:10.1016/j.foreco.2013.05.030.

Yang, X.D., et al., 2019. Surface functional groups of carbon-based adsorbents and their roles in the removal of heavy metals from aqueous solutions: A critical review. *Chemical Engineering Journal*, 366, 608–621. doi:10.1016/j.cej.2019.02.119.

Yeh, T., 2006. *Chemical and structural characterizations of juvenile wood, mature wood, and compression wood of loblolly pine (Pinus taeda)*. Raleigh, NC: North Carolina State University.

Yu, J., et al., 2018. Influence of temperature and particle size on structural characteristics of chars from beechwood pyrolysis. *Journal of Analytical and Applied Pyrolysis*, 130, 127–134. doi:10.1016/j.jaap.2018.01.018.

Zamora-Ledezma, C., et al., 2021. Heavy metal water pollution: A fresh look about hazards, novel and conventional remediation methods. *Environmental Technology & Innovation*, 22, doi:10.1016/j.eti.2021.101504.

Zhou, Q.Q., et al., 2020. Total concentrations and sources of heavy metal pollution in global river and lake water bodies from 1972 to 2017. *Global Ecology and Conservation*, 22, doi:10.1016/j.gecco.2020.e00925.